Systems-level identification of PKA-dependent signaling in epithelial cells

Kiyoshi Isobe[a], Hyun Jun Jung[a], Chin-Rang Yang[a], J'Neka Claxton[a], Pablo Sandoval[a], Maurice B. Burg[a], Viswanathan Raghuram[a], and Mark A. Knepper[a,1]

[a]Epithelial Systems Biology Laboratory, Systems Biology Center, National Heart, Lung, and Blood Institute, National Institutes of Health, Bethesda, MD 20892-1603

Edited by Peter Agre, Johns Hopkins Bloomberg School of Public Health, Baltimore, MD, and approved August 29, 2017 (received for review June 1, 2017)

G protein stimulatory α-subunit ($G_{\alpha s}$)-coupled heptahelical receptors regulate cell processes largely through activation of protein kinase A (PKA). To identify signaling processes downstream of PKA, we deleted both PKA catalytic subunits using CRISPR-Cas9, followed by a "multiomic" analysis in mouse kidney epithelial cells expressing the $G_{\alpha s}$-coupled V2 vasopressin receptor. RNA-seq (sequencing)–based transcriptomics and SILAC (stable isotope labeling of amino acids in cell culture)-based quantitative proteomics revealed a complete loss of expression of the water-channel gene *Aqp2* in PKA knockout cells. SILAC-based quantitative phosphoproteomics identified 229 PKA phosphorylation sites. Most of these PKA targets are thus far unannotated in public databases. Surprisingly, 1,915 phosphorylation sites with the motif x-(S/T)-P showed increased phosphooccupancy, pointing to increased activity of one or more MAP kinases in PKA knockout cells. Indeed, phosphorylation changes associated with activation of ERK2 were seen in PKA knockout cells. The ERK2 site is downstream of a direct PKA site in the Rap1GAP, Sipa1l1, that indirectly inhibits Raf1. In addition, a direct PKA site that inhibits the MAP kinase kinase kinase Map3k5 (ASK1) is upstream of JNK1 activation. The datasets were integrated to identify a causal network describing PKA signaling that explains vasopressin-mediated regulation of membrane trafficking and gene transcription. The model predicts that, through PKA activation, vasopressin stimulates AQP2 exocytosis by inhibiting MAP kinase signaling. The model also predicts that, through PKA activation, vasopressin stimulates *Aqp2* transcription through induction of nuclear translocation of the acetyltransferase EP300, which increases histone H3K27 acetylation of vasopressin-responsive genes (confirmed by ChIP-seq).

CRISPR-Cas9 | phosphoproteomics | vasopressin | protein mass spectrometry | next-generation sequencing

Heptahelical receptors that couple to the G protein stimulatory α-subunit ($G_{\alpha s}$) regulate cell processes largely through activation of protein kinase A (PKA). In a subset of G protein-coupled receptors (GPCRs), ligand binding results in activation of the heterotrimeric $G_{\alpha s}$, which activates adenylyl cyclases and increases intracellular cyclic AMP (cAMP). These $G_{\alpha s}$-coupled receptors include those that regulate glycogenolysis in the liver (glucagon and epinephrine), hydrolysis of triglycerides in adipose tissue (epinephrine), secretion of thyroid hormone (thyroid-stimulating hormone), synthesis of steroid hormones in the adrenal cortex (adrenocorticotropic hormone), resorption of bone (parathyroid hormone), contractility and rate of contraction in the heart (epinephrine), and water excretion by the kidney (vasopressin) (2). Foremost among effectors of cAMP is PKA, also known as cAMP-dependent protein kinase (3, 4). PKA is a basophilic S/T kinase in the AGC family (5) that phosphorylates serines and threonines in target proteins that possess basic amino acids (R>K) at positions −3 and −2 relative to the phosphorylation site [PKA target motif: (R/K)-(R/K)-x-(pS/pT), where x is any amino acid] (6–8). Lists of protein targets of PKA, identified in reductionist studies, have been curated in databases such as Phospho.ELM (9), the Human Protein Reference Database (10), PhosphoNET (11), and PhosphoSitePlus (12), although it is likely that many direct PKA targets are as yet unidentified. Some of the known PKA targets are other protein kinases and phosphatases, meaning that PKA activation is likely to result in indirect changes in protein phosphorylation manifest as a signaling network, the details of which remain unresolved. To identify both direct and indirect targets of PKA in mammalian cells, we used CRISPR-Cas9 genome editing to introduce frame-shifting indel mutations in both PKA catalytic subunit genes (*Prkaca* and *Prkacb*), thereby eliminating PKA-Cα and PKA-Cβ proteins. This was followed by use of quantitative (SILAC-based) phosphoproteomics to identify phosphorylation sites whose phosphooccupancies are altered by the deletions. Beyond this, we used additional large-scale methodologies [RNA-seq (sequencing), ChIP-seq for histone H3 lysine-27 acetylation, and standard SILAC-based quantitative protein mass spectrometry] to pinpoint downstream effects of PKA deletion associated with changes in gene transcription and protein expression.

To do these studies, we used a cell line (mouse *mpkCCD*) expressing the $G_{\alpha s}$-coupled vasopressin receptor V2R (gene: *Avpr2*) that mediates the action of the peptide hormone vasopressin in the regulation of osmotic water transport in the kidney (13). These cells grow well and are readily transfected, and yet they manifest differentiated functions that closely mimic native renal collecting duct principal cells (14–16). Thus, they provide a model system conducive to genome editing, but with a turnover

Significance

Maintenance of homeostasis is dependent on intercellular communication via secreted hormones that bind G protein-coupled receptors. Many of these receptors activate an enzyme called protein kinase A (PKA) that modifies cell function by covalently attaching phosphate groups to proteins. To comprehensively identify PKA substrates, we used genome editing (CRISPR-Cas9) to delete PKA from kidney epithelial cells followed by large-scale mass spectrometry to measure phosphorylation changes throughout the proteome; 229 PKA target sites were identified, many previously unrecognized. Surprisingly, PKA deletion caused seemingly paradoxical phosphorylation increases at many sites, indicating secondary activation of one or more mitogen-activated kinases. The data, coupled with transcriptomics and standard proteomics, identified a signaling network that explains the effects of PKA that regulate cellular functions.

Author contributions: M.B.B., V.R., and M.A.K. designed research; K.I., H.J.J., C.-R.Y., J.C., and P.S. performed research; K.I., H.J.J., C.-R.Y., V.R., and M.A.K. analyzed data; and K.I., H.J.J., C.-R.Y., J.C., P.S., M.B.B., V.R., and M.A.K. wrote the paper.

The authors declare no conflict of interest.

This article is a PNAS Direct Submission.

Data deposition: The protein mass spectrometry data (raw files, search results, and spectra) reported in this paper have been deposited in the ProteomeXchange Consortium via the PRIDE partner repository, www.ebi.ac.uk/pride/archive (ID code PXD005938). The FASTQ sequences and metadata for the RNA-seq and ChIP-seq studies reported in this paper have been deposited in the Gene Expression Omnibus (GEO) database, https://www.ncbi.nlm.nih.gov/geo (accession no. GSE95009).

[1]To whom correspondence should be addressed. Email: knepperm@nhlbi.nih.gov.

This article contains supporting information online at www.pnas.org/lookup/suppl/doi:10.1073/pnas.1709123114/-/DCSupplemental.

rate compatible with efficient metabolic labeling of proteins required for SILAC quantification. These cells manifest vasopressin responses characteristic of native renal principal cells, including vasopressin-induced increases in adenylyl cyclase activity (14), vasopressin-induced trafficking of the molecular water channel aquaporin-2 (AQP2) to the plasma membrane (15), vasopressin-induced increase in AQP2 protein stability (17), and vasopressin-induced increases in transcription of the *Aqp2* gene (16, 18).

The studies identified 229 phosphorylation sites in 197 proteins that showed decreased phosphooccupancy in cells with CRISPR-Cas9 deletion of PKA-Cα and PKA-Cβ, including 47 sites in which phosphorylation was ablated by more than 90%. Many of these PKA target sites are previously unidentified as PKA substrates. Furthermore, there were many phosphorylation sites with increased phosphooccupancy that possessed a proline at position +1 relative to the phosphorylated amino acid. This indicates that the PKA deletion secondarily activates one or more MAP kinases or cyclin-dependent kinases. An ancillary finding was that expression of the *Aqp2* gene is absolutely dependent on PKA. Using large-scale data integration techniques, the quantitative proteomic, phosphoproteomic, RNA-seq, and ChIP-seq datasets obtained in this study were integrated with prior data from the literature to identify a PKA signaling network that has been curated online as a publicly accessible resource (https://hpcwebapps.cit.nih.gov/ESBL/PKANetwork/). This network links direct PKA targets to the known physiological responses to V2R signaling.

Results

To eliminate functional PKA protein, we used CRISPR-Cas9 to create indel mutations in exons corresponding to the catalytic regions of PKA-Cα and PKA-Cβ in mouse mpkCCD cells (Fig. 1*A*). Three distinct guide (g)RNAs were used for both genes, each producing multiple clonal cell lines. Double-knockout (dKO) lines were created using the PKA-Cβ knockout cell lines and superimposing PKA-Cα mutations (Fig. 1*B*). We raised isoform-specific antibodies targeting epitopes upstream of the catalytic domains and carried out Western blotting analysis revealing an absence of the respective PKA catalytic subunit proteins in single- and double-KO lines (Fig. 1*C*). Cell lines from CRISPR experiments that retained expression of PKA were used as control lines (Fig. 1*B*, control A and control B, blue) for subsequent experiments. Among all available dKO and control lines, three representative dKO/control pairs were chosen for further studies. DNA sequencing (PCR/Sanger) identified specific indel mutations in *Prkaca* and *Prkacb* of the dKO lines and demonstrated a lack of PKA mutations in the control lines (Table S1).

PKA dKO Cells Are Viable and Retain Epithelial Structure and Function. All dKO lines were viable, and grew at approximately the same rates as control cells. The dKO cells exhibited intact epithelial organization, as evidenced by immunofluorescence localization of the tight junction marker ZO-1 and the basolateral plasma membrane marker Na^+-K^+-ATPase (Fig. 1*D*). ZO-1 labeling at the tight junctions was sustained, but appeared to be decreased in the PKA dKO cells with increased ZO-1 labeling in the cell nuclei. Transepithelial resistance values increased to high levels on day 1 after seeding as the cells became confluent (Fig. 1*E*). Interestingly, the transepithelial resistance values were moderately lower in the PKA dKO cells relative to controls. We conclude that the PKA dKO cells are viable and retain their epithelial architecture, and the ion permeability of the tight junctions appears to be a possible target of PKA-dependent regulation.

We carried out Western blotting for aquaporin-2 in multiple PKA-Cα and PKA-Cβ single-knockout lines as well as multiple dKO lines along with the respective controls (Fig. 2 *A*–*H*). Both single knockouts resulted in a reduction in AQP2 protein abundance, although AQP2 abundance was decreased more in the PKA-Cα single-KO clones (Fig. 2*B*) than in PKA-Cβ single-KO clones (Fig. 2*E*). In the PKA dKO cells, AQP2 protein was undetectable, indicating that AQP2 protein expression requires PKA (Fig. 2 *G* and *H*). Interestingly, knocking out PKA-Cα resulted in

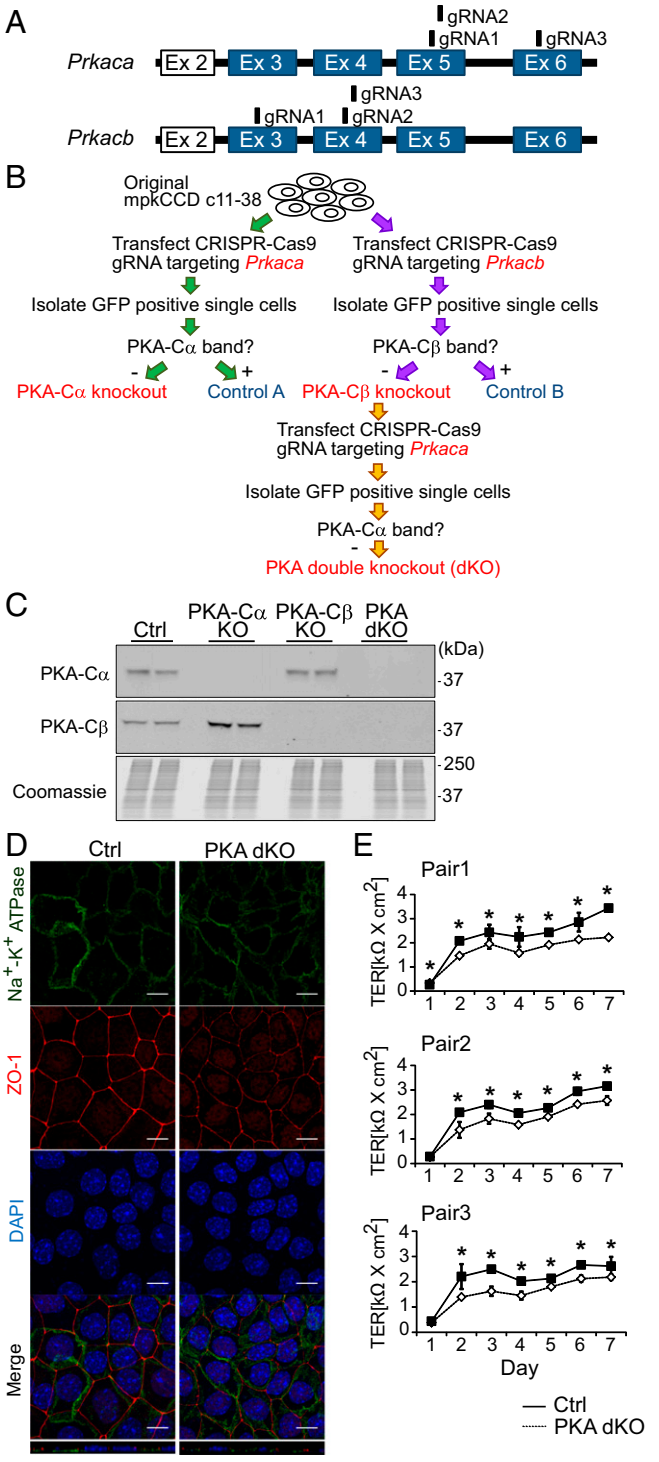

Fig. 1. Establishment and characterization of PKA-Cα single knockout, PKA-Cβ single-knockout, and PKA double-knockout cell lines. (*A*) Location of sequences targeted by guide RNAs in mouse *Prkaca* and *Prkacb* genes. Exons that code for catalytic domains are shown in blue. Ex, exon. (*B*) Flowchart for the generation of PKA dKO cell lines. Clones that have target gene expression and no detectable mutation were used as controls (blue) for the respective knockout clones (red). Three pairs of dKO clones and their respective control clones were selected for subsequent experiments. (*C*) Representative Western blots for PKA-Cα and PKA-Cβ proteins. (*D*) Immunofluorescence images showing a basolateral marker (Na^+-K^+ ATPase) and a tight junction marker (ZO-1) in PKA dKO and control cells. Merged images include both *x*–*y* (*Top*) and *x*–*z* (*Bottom* thin panels) perspectives. (Scale bars, 10 μm.) (*E*) Transepithelial resistance (TER) versus time after plating for three pairs of PKA dKO and control cells. Values are mean ± SD (n = 6, *P < 0.05, Student t test).

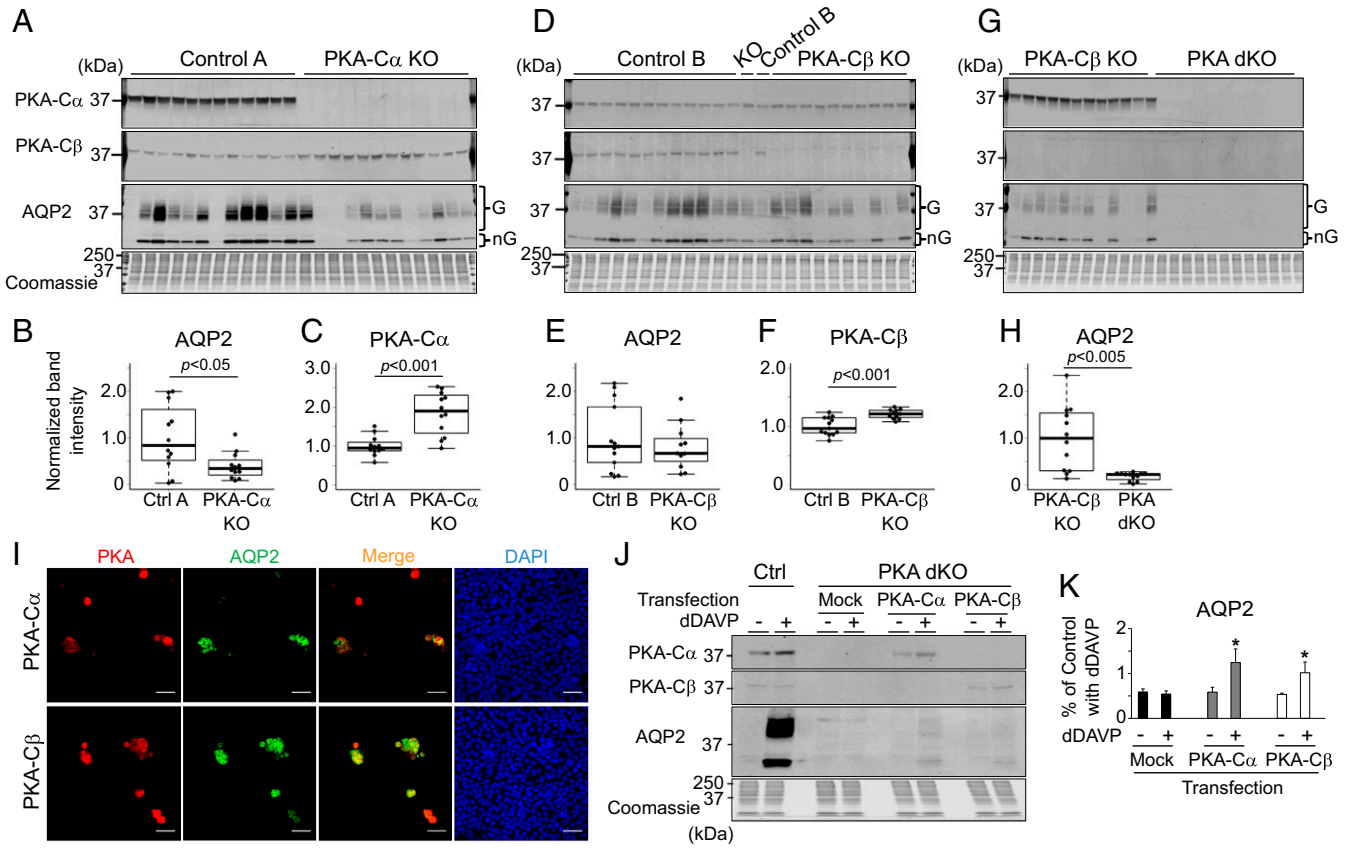

Fig. 2. AQP2 abundance in PKA knockout cells and its rescue by PKA. All observations were made in the presence of dDAVP (0.1 nM continuously). (*A*, *D*, and *G*) Western blots for PKA-Cα, PKA-Cβ, and AQP2 are shown for 12 control clones versus 12 PKA-Cα knockout clones (*A*), 13 control clones versus 11 PKA-Cβ knockout clones (*D*), and 12 control clones versus 12 PKA dKO (*G*). Loading: PKA-Cα blots, 20 μg; PKA-Cβ blots, 30 μg; AQP2 blots, 10 μg; Coomassie, 7 μg. G, glycosylated; nG, nonglycosylated. (*B*, *C*, *E*, *F*, and *H*) Band density quantification of the respective immunoblots using beeswarm plus boxplot visualization. Each point is a quantification of a single lane. The heavy horizontal lines represent the median. Band density for AQP2 is summed for glycosylated and nonglycosylated bands. Band densities were normalized by the mean of respective control observations. (*I*) Immunofluorescence images showing that clusters of PKA dKO cells transfected with PKA-Cα or PKA-Cβ plasmids express AQP2 protein. DAPI labeling shows that the cells are confluent. (Scale bars, 30 μm.) (*J* and *K*) Western blot (*J*) and quantification (*K*) of protein abundance in transfected cells ($n = 3$, mean ± SD, $^*P < 0.05$). Values are normalized by band density of AQP2 in vasopressin-treated control cells and expressed as a percentage. Loading: PKA-Cα blots, 20 μg; PKA-Cβ blots, 30 μg; AQP2 blots, 60 μg; Coomassie, 7 μg.

a marked increase in PKA-Cβ protein (Fig. 2 *A* and *C*). Similarly, knocking out PKA-Cβ resulted in an increase in PKA-Cα protein, although the effect was less pronounced (Fig. 2 *D* and *F*). Both findings point to potential compensatory responses.

Rescue of AQP2 Protein Expression by Transfection of Prkaca or Prkacb in PKA dKO Cells. To further address the role of PKA in the regulation of AQP2 protein abundance, we carried out rescue experiments in which PKA dKO cells were transfected with plasmids to express either PKA-Cα or PKA-Cβ (Fig. 2 *I*–*K*). As shown by immunofluorescence labeling of vasopressin-treated cells in Fig. 2*I*, cell clusters expressing either of the two transfected catalytic subunits had variable (but readily detectable) AQP2 protein, while other cells in the same monolayer that did not express PKA protein did not have detectable AQP2. Fig. 2 *J* and *K* show corresponding Western blotting results for additional rescue experiments. Despite a relatively low transfection efficiency, AQP2 was readily detectable after transfection with either PKA catalytic subunit when the cells were exposed to vasopressin. We conclude that the vasopressin-mediated increase in AQP2 protein abundance requires PKA.

RNA-Seq. Next, we asked two questions: (*i*) "Is the loss of AQP2 protein in the PKA dKO cells associated with loss of *Aqp2* mRNA?" and (*ii*) "what other genes show changes in expression with PKA deletion?" To address these questions, we carried out RNA-seq in three PKA dKO clones vs. three separate control clones with intact expression of PKA (Fig. 3 *A* and *B*). As shown in Fig. 3*A*, reads corresponding to *Aqp2* transcripts were virtually absent in the PKA dKO cells (*Upper Left*). Thus, the absence of AQP2 protein is due to an absence of *Aqp2* mRNA. Fig. 3*A* also shows examples of mapped reads for additional transcripts, namely *Prkaca* (markedly decreased), *Prkacb* (unchanged), the vasopressin receptor *Avpr2* (relatively unchanged), *Marcks* (increased), and *Rhcg* (increased). The decrease in *Prkaca* mRNA could be due to a decrease in the stability of the mutant mRNA or to a physiological effect on transcription. The latter possibility could be seen, for example, if PKA protein were required for *Prkaca* gene transcription in a manner similar to its role in regulation of *Aqp2* gene transcription. The full dataset (Dataset S1) is summarized in Fig. 3*B*. Most mRNA species were relatively unchanged in abundance. Interestingly, the mRNA for *Aqp2* stood out as the most profoundly suppressed transcript among all 10,190 quantified. Thus, PKA is required for *Aqp2* gene expression. Transcripts with false discovery rate (FDR) <0.05 are indicated by red points ($n = 354$). In Fig. 3*B*, only transcripts with FDR <0.05 and $|\log_2(\text{dKO/ctrl})| > 2$ are labeled. Both myristoylated alanine-rich C-kinase substrate (*Marcks*) and the ammonia transporter (*Rhcg*) matched this criterion and were increased in abundance. Nine transcripts matched this criterion and were decreased, namely *Aqp2*, *Prkaca*, *Pde4b*, *Zhx2*, *Gsdmc2*, *Gsdmc4*, *Cd55*, *Adh1*, and *Tmprss4*. In collecting duct cells, Tmprss4 has been identified as an activator of the epithelial sodium channel

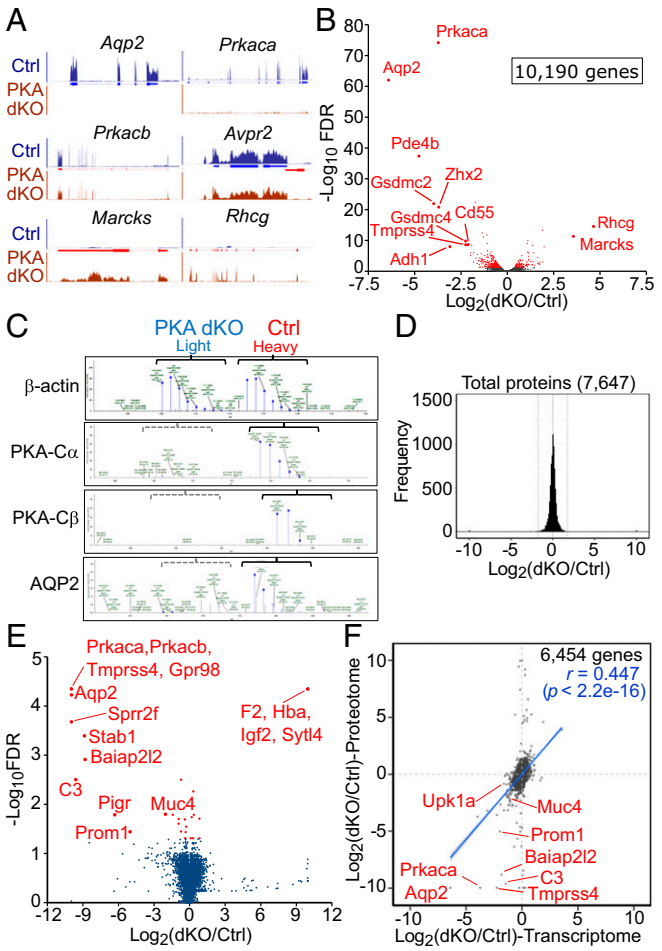

Fig. 3. RNA-seq–based transcriptomic and SILAC-based quantitative proteomic analysis of PKA dKO versus control cells. (*A*) Distribution of RNA-seq reads across gene bodies of selected genes for one PKA dKO/control pair: *Aqp2* (decreased), *Prkaca* (decreased), *Prkacb* (unchanged), *Avpr2* (unchanged), *Marcks* (increased), and *Rhcg* (increased). Reading direction: blue, left to right; red, right to left. The vertical axis shows binned read counts normalized by total read number (read counts per 10^7). (*B*) Volcano plot for 10,190 transcripts expressed in control and PKA dKO cells, quantified for three pairs of PKA dKO vs. control clones. Red points are transcripts with FDR <0.05. Labeled transcripts are discussed in the text. (*C*) MS1 spectra of representative β-actin, PKA-Cα, PKA-Cβ, and AQP2 peptides showing peaks for control cells (labeled with heavy amino acids) and PKA dKO cells (labeled with light amino acids). Dashed brackets indicate the expected (but not observed) peak locations in the PKA dKO cells (light). The vertical axis shows peptide ion intensity, and the horizontal axis shows the mass-to-charge ratio (*m/z*). Each peptide has several *m/z* peaks due to the presence of natural isotopes. (*D*) The distribution of protein abundance changes for 7,647 proteins in PKA dKO versus control cells ($n = 3$ pairs). The horizontal axis shows the median $\log_2$ (dKO/Ctrl) over the three determinations. Vertical dashed lines indicate mean and ±2 SD (mean, −0.02; SD, 0.87). (*E*) Volcano plot for the 7,647 proteins quantified in all three pairs of samples. Red points indicate proteins with FDR <0.05. Proteins with FDR <0.05 and absolute value of $\log_2$ (dKO/Ctrl) >2 are labeled with the official gene symbol. (*F*) Correlation between changes in transcript abundance (RNA-seq) and protein abundance (SILAC) in PKA dKO versus control cells. Genes with FDR <0.05 in both analyses are labeled with the official gene symbol. The blue line shows linear regression (with ±SE in gray) calculated from all data.

(19), a key protein in the regulation of blood pressure. Among these transcripts, several were previously found to increase in response to vasopressin in mpkCCD cells, namely *Aqp2*, *Pde4b*, *Gsdmc2*, *Adh1*, *Gsdmc4*, and *Tmprss4* (18, 20). Based on these observations, we conclude that PKA signaling is important for expression of a limited number of genes in addition to *Aqp2*. RNA-seq data are curated in Genome Browser format at https://hpcwebapps.cit.nih.gov/ESBL/Database/PKA-KO/.

SILAC-Based Quantitative Proteomics. Next, we asked, "What proteins, aside from AQP2, show changes in abundance in the PKA dKO cells versus control?" For this, we carried out protein mass spectrometry (LC-MS/MS) using SILAC (stable isotope labeling of amino acids in cell culture) (21) for quantification (Fig. 3 *C*–*F*). Fig. 3*C* shows examples of MS1 spectra. They confirm the absence of PKA-Cα and PKA-Cβ protein in the PKA dKO cells, and also confirm the profound decrease in AQP2 protein. In contrast, β-actin abundance was virtually unchanged. Among the 7,647 proteins quantified in all three biological replicates, abundances of most were relatively unchanged (Fig. 3*D*). Fig. 3*E* is a volcano plot in which only proteins with FDR <0.05 (red points) and $|\log_2(\text{dKO/ctrl})| > 2$ are labeled (Dataset S2). The data confirm the profound decrease in AQP2 protein in the PKA dKO cells demonstrated previously by Western blotting. Fig. 3*F* compares the mRNA responses from the RNA-seq data with protein responses from the quantitative mass spectrometry data (three replicates) (Dataset S3). Surprisingly, there was a broad correlation between the change in transcript abundance and the change in protein abundance ($R = 0.445$, $P < 2.2 \times 10^{-16}$), even among those with relatively small changes, indicating that PKA deletion has a broad effect across the expressed transcriptome. The gene products labeled in red are those with FDR <0.05 for both measures. Again, aquaporin-2 changes were greatest among all gene products quantified by both measures. Note also that a few proteins showed large changes in abundance in the PKA dKO without changes in transcript abundance, presumably due to selective regulation of translation or to selective control of protein stability.

Quantitative Phosphoproteomics. To identify signaling events downstream of PKA, we carried out SILAC-based quantitative phosphoproteomics in three distinct PKA dKO clones paired with control clones in which PKA was not deleted (Fig. 4); 13,913 phosphopeptides were quantified in at least two of three dKO/control pairs and 9,936 were quantified in all three pairs (Dataset S4). Most quantified phosphopeptides showed no substantial change in abundance (Fig. 4*A*). Among the phosphorylation sites found to be decreased [dKO/control (ctrl) <0.6], there was a predominance of sites with arginine (R) or lysine (K) in position −3 relative to the phosphorylated amino acid, indicating decreased phosphorylation by one or more basophilic protein kinases (AGC or CAMK families; Fig. 4*A*, *Upper Left*). The pattern seen here resembles that seen for phosphorylation events resulting from incubation of protein mixtures with recombinant PKA, including the preference for amino acids with branched-chain aliphatic side chains in position +1 (8).

Among phosphorylation sites found to be increased (dKO/ctrl >1/0.6 = 1.667), there was a predominance of sites with proline (P) in position +1, indicating increases in phosphorylation by proline-directed kinases (CMGC family), which include mitogen-activated protein kinases (MAPKs) and cyclin-dependent protein kinases (Fig. 4*A*, *Upper Right*). This finding is consistent with the view that one or more proline-directed kinases are negatively regulated either directly or indirectly by PKA in renal epithelial cells (22). Fig. 4*B* shows the distributions of amino acid sequence motifs among the phosphopeptides decreased in the PKA dKO cells (*Upper*) and increased in the PKA dKO cells (*Lower*). Among those decreased, 33.2% had arginine or lysine in position −3 (basophilic targets). Among those increased in the PKA dKO, 53.4% had proline in position +1 (CMGC targets).

We next asked the question, "Do phosphorylation sites that nominally fit the model for PKA targets [motif R-(R/K)-X-pS] get phosphorylated by PKA if the site is also a nominal proline-directed site with proline in position +1?" The answer as revealed in Fig. 4*C* is that proline in position +1 appears to block PKA-mediated phosphorylation. Specifically, none of the sites with the motif R-(R/K)-X-pS-P (nominally basophilic with proline in position +1) showed profound decreases in phosphorylation in the PKA dKO

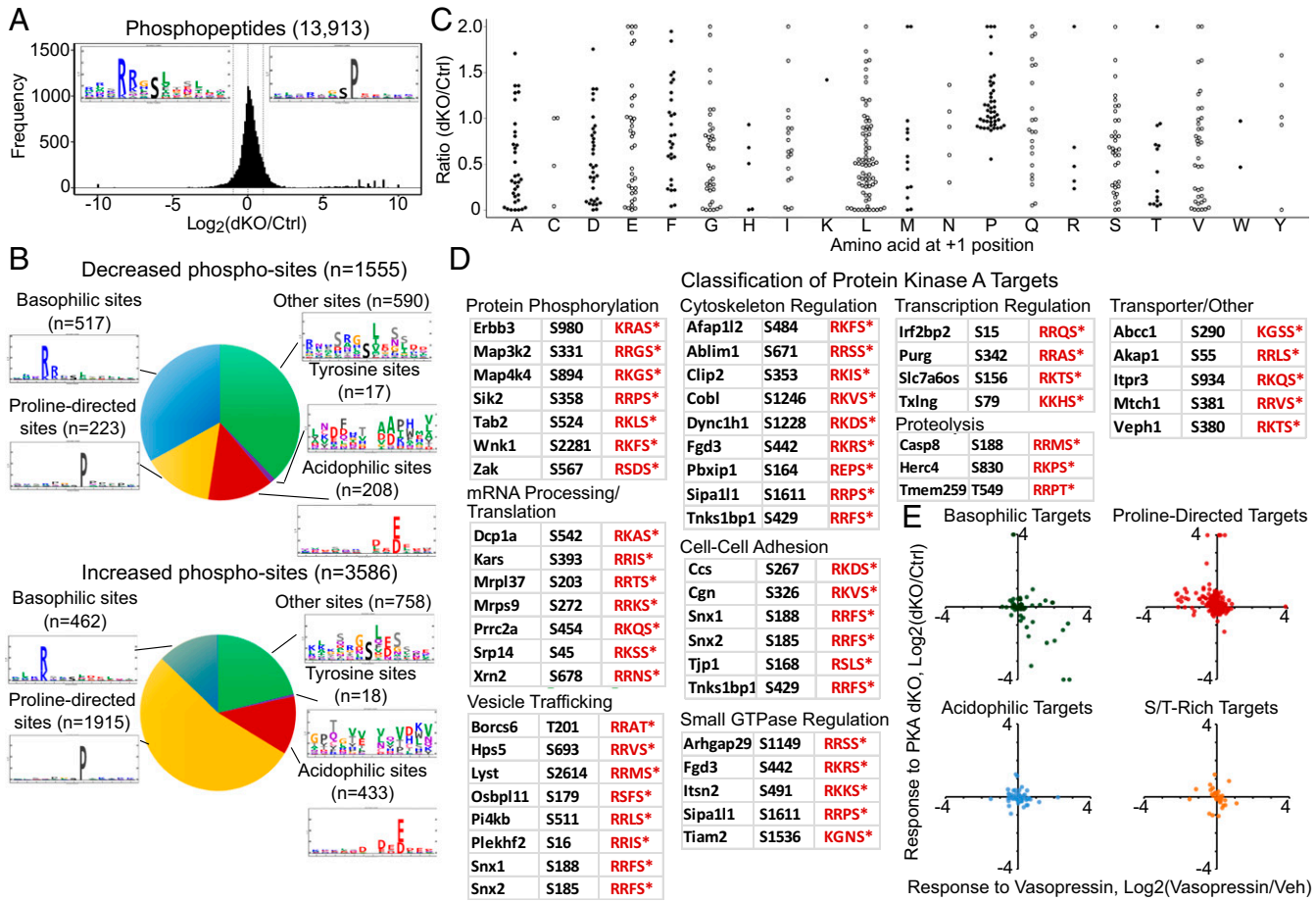

Fig. 4. Phosphorylation-site analysis of PKA dKO by LC-MS/MS. (*A*) Distribution of changes for phosphopeptides quantified in at least two pairs (13,913 phosphopeptides). Vertical dashed lines show $\log_2$(dKO/Ctrl) of 0, +1, and −1. Median $\log_2$(dKO/ctrl) = 0.16. Logos summarize the sequence patterns for phosphopeptides that are decreased (*Upper Left*) or increased (*Upper Right*) by more than 40%. The former shows a dominance of basophilic kinases (ACG and CAMK families), while the latter shows a dominance of proline-directed kinases (CMGC family). (*B*) Classification of decreased (*Upper*) and increased (*Lower*) phosphorylation sites according to sequence patterns. For the purposes of this analysis, basophilic sites are defined as those with arginine or lysine at position −3; proline-directed sites are defined as those with proline at position +1; and acidophilic sites are defined as those with aspartic acid or glutamic acid at position +3 with respect to the phosphorylated amino acid. (*C*) Analysis of basophilic phosphopeptides with various amino acids at position +1. Beeswarm plots of mean phosphopeptide ratio of dKO/Ctrl versus amino acid at position +1. Each point represents a phosphopeptide ratio for one phosphopeptide. (*D*) List of direct PKA targets. Phosphopeptides which were decreased by at least 90% in PKA dKO and contain arginine or lysine at position −3 are defined as likely exclusive direct PKA target sites. These sites are listed by molecular function, giving gene symbol, target amino acid, and four-amino acid sequence, with an asterisk indicating the phosphorylated amino acid. (*E*) Change in phosphorylation in response to PKA dKO among sites previously identified as vasopressin-regulated phosphorylation sites. Phosphorylation sites are classified in motif categories: basophilic sites, proline-directed sites, acidophilic sites, and S/T-rich sites. S/T-rich sites contain serine or threonine at position +1 or −1 and were not in the other categories.

cells. Among the basophilic sites with decreased phosphorylation in the PKA dKO cells, 47 showed decreases of >90%, and are here considered to be likely direct targets of PKA (Dataset S5). Some could be indirect targets of PKA, due to PKA-mediated activation of other basophilic protein kinases. Additionally, the phosphoproteomic analysis identified 182 basophilic sites that showed lesser decreases in phosphooccupancy in the PKA dKO cells (0.1< dKO/ctrl <0.6) (Dataset S5). Many of these are also likely PKA sites that presumably can also be phosphorylated by other basophilic protein kinases that were not deleted (e.g., protein kinase G or calmodulin-dependent kinase II). They include several known PKA target sites including Ser552 of β-catenin (Ctnnb1), Ser104 of cAMP-regulated phosphoprotein 19 (Arpp19), Ser885 of Rho guanine nucleotide exchange factor 2 (Arhgef2), Ser155 of Bcl2-associated agonist of cell death (Bad), and Ser1406 of aspartate carbamoyltransferase (Cad) (cf. PhosphoSitePlus and Phospho.ELM databases). These proteins are distributed among several functional categories relevant to the physiological actions of vasopressin in collecting duct cells (Fig. 4*D*). Among the PKA target substrates, four protein kinases were identified with decreased phosphorylation in the PKA dKO cells at sites that are known from prior evidence to affect their enzymatic activity, namely Ser358 of Sik2 (salt-inducible kinase 2), Ser17 of Src, Ser2448 of mTOR, and Ser973 of Map3k5 (cf. Kinexus PhosphoNET database). These form the core of a proposed PKA signaling network (see below). Note in addition that there were multiple phosphorylation sites that decreased in the PKA dKO cells but did not possess upstream amino acids compatible with phosphorylation by PKA (Fig. 4*B*), including several protein kinases (Table S2). These sites are presumably downstream of but not direct targets of PKA.

In a previous study, we used SILAC to quantify phosphoproteomic responses to vasopressin in mpkCCD cells (22). Of the 853 phosphorylation sites quantified in that study, 458 phosphorylation sites were also quantified in the PKA dKO cells in the present study. Fig. 4*E* compares these values for phosphorylation sites categorized into four general categories by kinase target motif. In general, a majority of sites showed little change by either measure. However, the distribution in the basophilic group skewed into the right lower quadrant, indicating that sites whose phosphorylation increased in response to vasopressin showed a corresponding

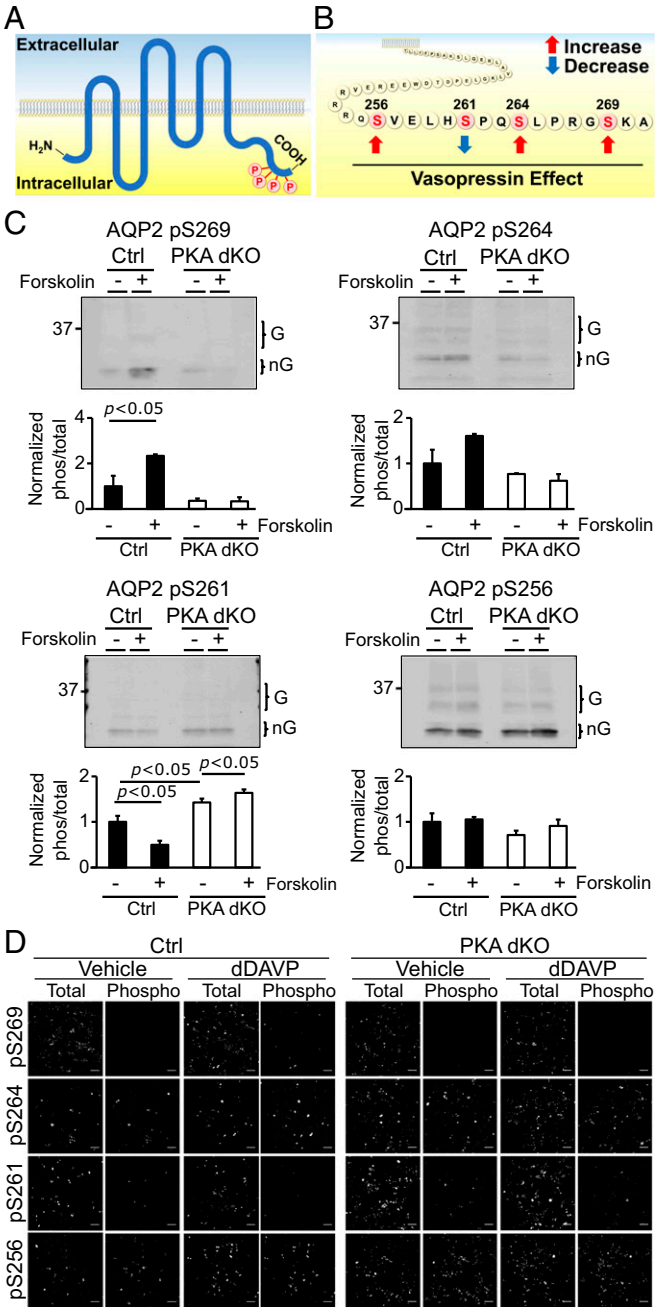

Fig. 5. Phosphorylation of aquaporin-2 in PKA dKO versus control mpkCCD cells. (*A*) AQP2 membrane-spanning topology. AQP2 has six transmembrane domains. A cluster of four vasopressin-dependent phosphorylation sites is present within the terminal 16 amino acids in the C-terminal tail. P, phosphorylation site. (*B*) The vasopressin-regulated phosphorylation sites are shown. Sequences surrounding Ser256, Ser264, and Ser269 are compatible with phosphorylation by basophilic protein kinases. Ser261 has a proline in position +1 and is presumably phosphorylated by a member of the MAPK family. Vasopressin decreases phosphorylation of Ser261 and increases phosphorylation at the other three sites. (*C*) Effect of PKA dKO on AQP2 phosphorylation levels. Both control and PKA dKO cells were transfected with AQP2, grown on a solid substratum for 24 h, and then treated with the adenylyl cyclase activator forskolin for 30 min ($n = 3$). Western blotting was done with phospho-specific antibodies recognizing each of the four phosphorylation sites (*Upper*) and quantified by densitometry (*Lower*). The bar graphs show normalized abundances as mean ± SD. Total AQP2 was quantified with a non–phospho-specific AQP2 antibody. (*D*) Low-power immunofluorescence images of total and phosphorylated AQP2 in PKA dKO and control cells. Cells were transfected with AQP2 and grown on a permeable support without dDAVP for 4 d. Subsequently, cells were stimulated with 0.1 nM dDAVP for 30 min. (Scale bars, 50 μm.)

decrease in phosphooccupancy in the PKA dKO. These sites were: Bad at S155, Cad at S1406, Ctnnb1 at S552, Fam83h at S970, Fam129a at S601, Golga5 at S116, Map3k2 at S153, Map4k5 at T400, Mcm2 at S21, Mtch1 at S381, Plekhg3 at S737, Reps1 at S272, Scyl2 at S677, Slc33a1 at S42, and Syne2 at S6371. Furthermore, the distribution in the proline-directed group skewed into the left upper quadrant, indicating that sites whose phosphorylation decreased in response to vasopressin showed a corresponding increase in phosphooccupancy in the PKA dKO (Fig. 4*E*). These phosphorylation sites were: Add3 at S681, Agfg1 at S181, Cnot2 at S165, Cxadr at S332, Dbnl at S291, Eps8l1 at T187, Eps8l2 at S483, Gprc5a at S344, Hdgf at T200, Limch1 at S973, Lrba at S979, Lrrc16a at S1295, Mcm2 at S27, Ppl at S14, Rab12 at S20, Slc9a3r1 at S275, and Tjp2 at S239. In contrast, changes in the acidophilic and S/T-rich groups were small and distributed symmetrically about the origin (Fig. 4*E*).

Phosphorylation of AQP2 in PKA Double KO. The water channel aquaporin-2 is phosphorylated on four serines within the carboxyl-terminal 16 amino acids (23) (Fig. 5*A*). Phosphorylation at each of these sites is regulated by vasopressin via increases in intracellular cAMP (24) (Fig. 5*B*). Because the PKA dKO cells did not express the *Aqp2* gene, assessment of the role of PKA in phosphorylation of these sites required transfection to express AQP2. Phosphorylation changes in AQP2 were assessed with phospho-specific antibodies (24) both by Western blotting (Fig. 5*C*) and by immunofluorescence (Fig. 5*D*). Phosphorylation at Ser269 of AQP2, a vasopressin-regulated site critical to the regulation of AQP2 endocytosis (24), was nearly undetectable in the PKA dKO cells and did not increase with the adenylyl cyclase activator forskolin (Fig. 5*C*, *Left*) or the vasopressin analog dDAVP (1-desamino-8-D-arginine-vasopressin) (Fig. 5*D*, *Top*) in contrast to the control cells with intact PKA. Thus, phosphorylation of AQP2 at Ser269 is PKA-dependent, although not necessarily by direct PKA-mediated phosphorylation. Phosphorylation at Ser264, a site normally increased in phosphooccupancy by vasopressin (24), is sustained in the PKA dKO cells, although it appears to be somewhat diminished and the increase that normally occurs in response to vasopressin did not occur. Because Ser264 of AQP2 is phosphorylated in the absence of PKA, we conclude that other kinases can phosphorylate it, although the response to vasopressin depends on PKA. Phosphorylation at Ser261 of AQP2, which normally decreases with vasopressin (23), was seen to be markedly increased in the PKA dKO cells, but did not decrease with forskolin or vasopressin, contrary to observations in the control cells with PKA. In fact, there was a small, but statistically significant, increase in Ser261 phosphorylation with forskolin in the PKA dKO cells (Fig. 5*C*), indicating the presence of a PKA-independent increase in the activity of one or more MAP kinases. Phosphorylation at Ser256 is seen with a high level of phosphooccupancy in either the absence or presence of vasopressin in mpkCCD cells (22) or native rat inner medullary collecting duct (IMCD) cells (25), and is generally regarded to be a PKA target based on the surrounding sequence, in vitro phosphorylation by PKA, and inhibition by PKA inhibitors, as discussed by Bradford et al. (26). Phosphorylation at this site was readily detectable in the PKA dKO cells and did not change with forskolin (Fig. 5*C*) or vasopressin (Fig. 5*D*). Thus, one or more basophilic protein kinases other than PKA can phosphorylate AQP2 at Ser256 in intact cells, that is, PKA is not obligatory for Ser256 phosphorylation. Previous studies have pointed to a role for one or more isoforms of calmodulin-regulated kinase 2 (CAMK2) in the phosphorylation of AQP2 at Ser256 in mpkCCD cells (27) and native rat IMCD cells (26). In additional experiments in the PKA-Cα and PKA-Cβ single knockouts, vasopressin-mediated phosphorylation changes in Ser269, Ser264, and Ser261 in endogenously expressed AQP2 were sustained, although attenuated in the PKA-Cα knockout cells (Fig. S1).

Functional Relevance of PKA-Mediated Signaling. The vasopressin V2 receptor-expressing cells of the kidney (collecting duct principal cells) have been comprehensively studied, revealing that several cellular physiological processes are regulated by vasopressin (Fig. 6*A*). We combined the data obtained in this study with prior evidence to build a PKA-dependent signaling network that lays out data-compatible mechanisms for the vasopressin-mediated functional responses. Components of the network, addressing each process in Fig. 6*A*, are shown in Fig. 6 *B–H*. The network can be viewed at a permanent publicly accessible website that provides documentation for each network element as "mouse-over" text (https://hpcwebapps.cit.nih.gov/ESBL/PKANetwork/). This network, while undoubtedly incomplete, provides a framework for future studies that will refine the model. In the following, we investigate a few key network components.

PKA-dependent transcriptional regulation. Vasopressin increases RNA polymerase II occupation across the body of the *Aqp2* gene, concomitant with an increase in *Aqp2* mRNA, pointing to a direct effect on *Aqp2* gene transcription (18). The subnetwork shown in Fig. 6*D* identifies six PKA targets that connect with documented downstream targets relevant to the regulation of *Aqp2* gene transcription, namely β-catenin (Ctnnb1), CREB (Creb1), salt-inducible kinase 2 (Sik2), GLI-Kruppel family member GLI3 (Gli3), nuclear factor of activated T cells cytoplasmic 2 (Nfatc2), and type 3 InsP3 receptor (Itpr3). Full documentation is given at https://hpcwebapps.cit.nih.gov/ESBL/PKANetwork/Transcription.html. One target is Nfatc2, which has previously been demonstrated to bind to an NFAT-binding motif that is located 489 bp upstream of the *Aqp2* transcription start site (28) and to regulate *Aqp2* gene expression (29). Its translocation into the nucleus is regulated by the phosphatase calcineurin via calcium signaling (30). Vasopressin causes calcium mobilization in collecting duct principal cells in the form of trains of aperiodic calcium spikes typical of Ca^{2+}-induced Ca^{2+} release channels. One such channel, Itpr3, is known to undergo PKA-mediated phosphorylation at Ser934 and Ser1832 (31). In the PKA dKO cells, these two sites showed a profound decrease in phosphorylation (Ser934, dKO/ctrl: 0.005; Ser1832, dKO/ctrl: 0.135). PKA phosphorylation at these sites is known to enhance InsP3-induced Ca^{2+} mobilization (32). PKA is also known to phosphorylate S358 of Sik2 (33), reducing its enzymatic activity (34) via 14-3-3 binding. In Sik2, two sites showed decreased phosphorylation in PKA dKO cells, namely Ser358 (dKO/ctrl: 0.043) and Ser587 (dKO/ctrl: 0.484). Downstream targets of Sik2 are two transcriptional coactivators, Crebbp and Ep300, as well as a CREB-regulated transcriptional coactivator (Crtc1 or Crtc2) (35). Sik2-mediated phosphorylation inhibits nuclear translocation of these coactivators (36). The network predicts that vasopressin working through PKA causes nuclear translocation of Nfatc2 (due to increased intracellular Ca^{2+}), Crebbp, and/or Ep300, as well as Crtc isoforms due to decreased Sik2 activity. Fig. 7*A* shows experiments that test these predictions, revealing a vasopressin-induced increase in nuclear Nfatc2, Crtc1, and Ep300 but not Crebbp. However, translocation of these factors is not seen in the PKA dKO cells.

Crebbp and Ep300 are histone acetyltransferases that acetylate histone H3 lysine-27, a histone mark associated with open chromatin and increased transcription (37). The translocation of Ep300 predicts that vasopressin, working through PKA, may increase histone H3K27 acetylation of some genes. We tested

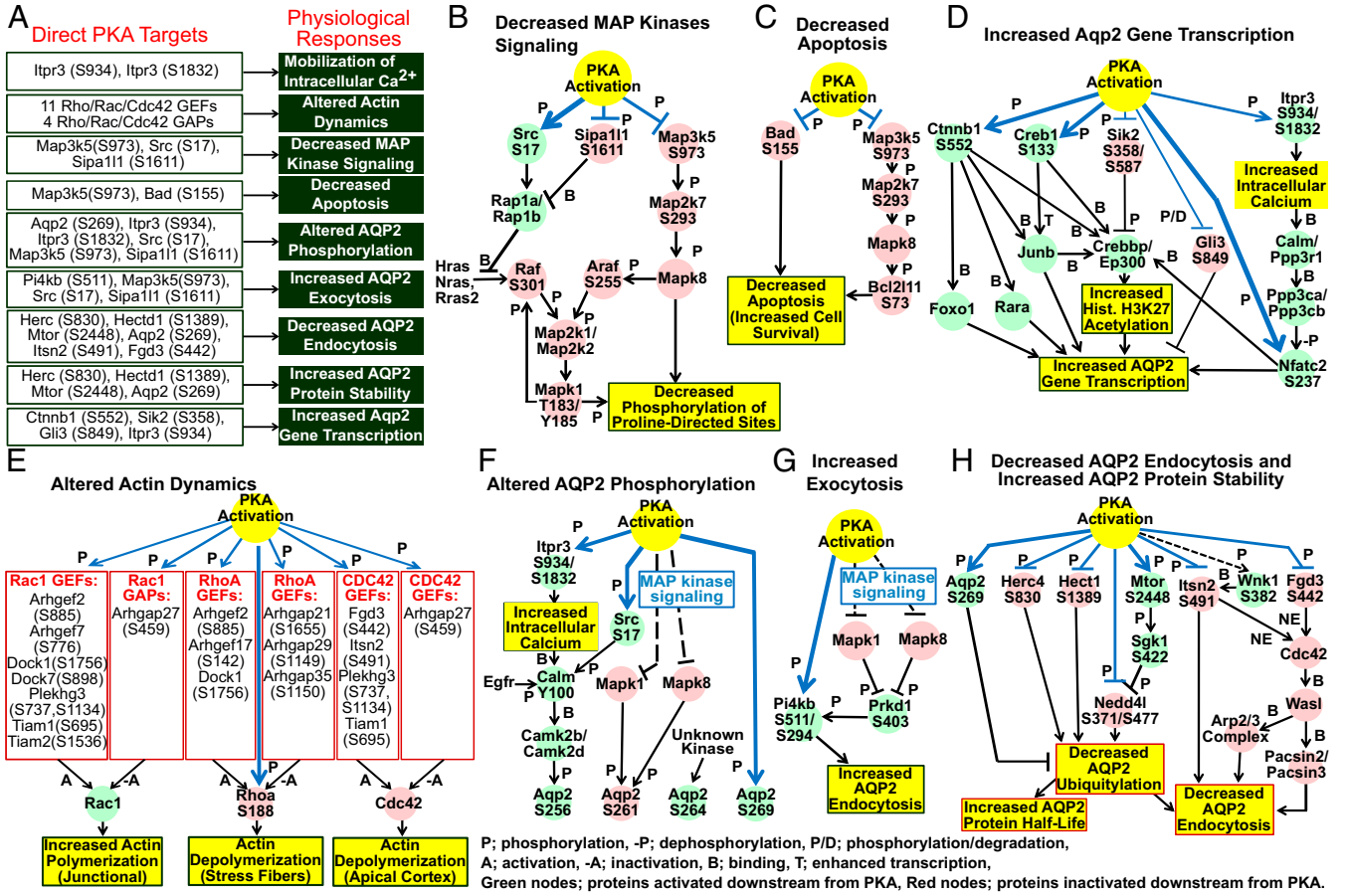

Fig. 6. PKA signaling mapped to functional effects of vasopressin. (*A*) Direct PKA targets and their physiological and functional effects. (*B–H*) PKA-regulated signaling network in MAP kinase signaling (*B*), decreased apoptosis (*C*), *Aqp2* gene transcription (*D*), actin dynamics (*E*), AQP2 phosphorylation (*F*), exocytosis (*G*), AQP2 endocytosis (*H*), and AQP2 protein stability (*H*). Data sources are given at https://hpcwebapps.cit.nih.gov/ESBL/PKANetwork/.

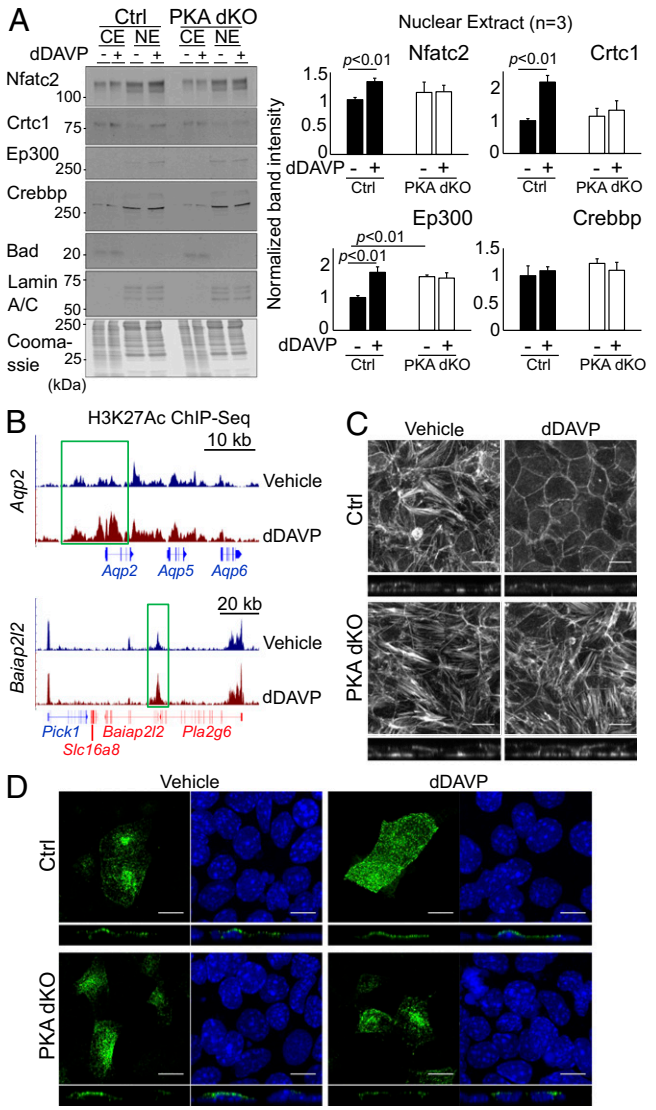

Fig. 7. Role of PKA in nuclear translocation of transcriptional regulators, histone acetylation, actin polymerization, and apical membrane trafficking of AQP2. (*A*) Nuclear translocation of transcriptional regulators in response to vasopressin. Western blot of nuclear and cytoplasmic extracts of various transcriptional regulators (*Left*). Densitometric analysis showing mean and SD (*Right*). CE, cytoplasmic extract; NE, nuclear extract. (*B*) Distribution of ChIP-seq reads across gene bodies of selected genes for vehicle- or dDAVP-treated cells. Green boxes highlight two genomic regions in which increases were observable. (*C*) Confocal projection *x–y* (*Top*) and *x–z* (*Bottom* thin panels) images showing changes in actin polymerization in response to vasopressin. Alexa-594 phalloidin staining in cells treated with vehicle or dDAVP. (Scale bars, 10 μm.) (*D*) Vasopressin-dependent AQP2 trafficking to the apical plasma membrane in control and PKA dKO cells. Confocal *x–y* (*Top*) and *x–z* (*Bottom* thin panels) images of cells treated with vehicle or dDAVP using anti-AQP2 antibody (green). DAPI-stained nuclei, blue. (Scale bars, 10 μm.)

this by performing ChIP-seq for this modification. As seen in Fig. 7*B*, there was a marked increase in histone H3K27 acetylation across the body of the *Aqp2* gene, and in the promoter, as well as in a region ~6,000 bp upstream of the *Aqp2* transcriptional start site. The adjacent *Aqp5* and *Aqp6* genes did not show parallel changes in histone H3K27 acetylation. Fig. 7*B*, *Lower* shows increased histone H3K27 acetylation for another vasopressin-induced gene, *Baiap2l2*, which is decreased in expression in the PKA dKO cells (compare Fig. 3*F*), while adjacent genes show no change. Examples of the H3K27Ac ChIP-seq data are displayed in Genome Browser format at https://hpcwebapps.cit.nih.gov/ESBL/Database/PKA-KO/.

PKA-dependent actin depolymerization. The small GTP-binding proteins Rho, Rac, and Cdc42 are involved in regulation of the state of actin polymerization. Prior studies have demonstrated that vasopressin causes actin depolymerization in both the apical cell cortex (38) and basal stress fibers in epithelial cells (39). The subnetwork shown in Fig. 6*E* identifies multiple Rho/Rac/Cdc42 GEFs and GAPs with phosphorylation sites that show decreased phosphooccupancy in the PKA dKO cells. These phosphoproteomic findings in the PKA dKO suggest that the actin-depolymerizing effects of vasopressin could be mediated by PKA. To test this, we carried out phalloidin labeling of control and PKA dKO cells, both in the presence and absence of the V2-receptor selective agonist dDAVP (Fig. 7*C*). dDAVP caused predominantly basal actin depolymerization in the control cells but not in the PKA dKO cells, supporting the hypothesis.

PKA-dependent AQP2 trafficking. Vasopressin regulates water permeability in the collecting duct by stimulating redistribution of the AQP2 water channel to the apical plasma membrane, thereby increasing the water permeability of collecting duct cells (40). Fig. 6 *G* and *H* shows that several PKA targets found in this study connect with the processes of exo- and endocytosis, namely Pi4kb (Ser511), Aqp2 (Ser269), Herc4 (Ser830), Hect1 (Ser1389), Nedd4l (Ser371, Ser477), Mtor (Ser2448), Itsn2 (Ser491), and Fgd3 (Ser442). These phosphoproteomic findings in the PKA dKO suggest that the effects of vasopressin on AQP2 trafficking to the apical plasma membrane could be mediated by PKA. To test this directly, we carried out immunocytochemical localization of AQP2 in control and PKA dKO cells transfected with AQP2 and challenged with either dDAVP or vehicle for 30 min (Fig. 7*D*). dDAVP caused translocation of AQP2 to the apical plasma membrane in the control cells but not in the PKA dKO cells, supporting the hypothesis.

Discussion

To identify signaling processes downstream of PKA activation, we have carried out quantitative proteomics, quantitative phosphoproteomics, ChIP-seq for chromatin modifications, and RNA-seq in epithelial cell lines in which both PKA catalytic subunits have been deleted using CRISPR-Cas9 genome editing. We have combined the current data with prior data to derive a signaling model that can explain the functional responses to GPCR activation by vasopressin in mammalian epithelial cells. Individual aspects of the model represent hypotheses, only a few of which we have addressed in the present paper. The model provides a framework not only for understanding how vasopressin regulates the function of kidney cells but likely overlaps PKA signaling pathways present downstream of other $G_{\alpha s}$-linked GPCRs. This network is provided as a permanent online resource that includes documentation for the nodes and edges revealed as popups, facilitating access to the original evidence.

A byproduct of the approach is an expanded list of phosphorylation target sites for protein kinase A, which is also provided as a permanent publicly accessible online resource. The identification of these targets greatly expands the list of known PKA substrates already documented in various databases. (Some known PKA targets were not detected, e.g., Ser188 of RhoA, whose tryptic peptide was likely too small to detect with the method used.) Beyond the direct targets of PKA, there was a large number of phosphorylation sites that showed increases in phosphooccupancy in the PKA double-knockout cells, most of them putative targets of MAP kinases, which phosphorylate serines or threonines with proline in position +1 relative to the phosphorylated amino acid. This result reveals that PKA activation in the present context inhibits MAP kinase signaling, consistent with findings of prior studies in epithelial cells (22, 41). This conclusion contrasts with several prior studies showing that some GPCRs increase MAP kinase signaling (42). The mechanism of activation of MAP kinases is incompletely understood, but is thought to be dependent on β-arrestin, protease-mediated EGF-receptor activation, or integrin-associated scaffolding by processes that are presumably not PKA-dependent. The general picture may be one of balanced effects on

MAP kinase signaling, with PKA-independent activation being opposed by PKA-dependent inactivation. Consistent with this, when PKA dKO cells were challenged with vasopressin, Ser261 of AQP2, an ERK2 substrate, showed a significant increase in phosphooccupancy, in contrast to the decrease seen with intact PKA.

In renal collecting duct cells, vasopressin regulates the water channel protein aquaporin-2 to control water excretion. It does so mainly by two mechanisms: (*i*) short-term effects to regulate trafficking and insertion of the AQP2 water channel into the plasma membrane (40), and (*ii*) long-term effects to alter AQP2 protein abundance largely through regulation of *Aqp2* gene transcription (43). The results of the present study demonstrate that PKA is required for both processes. With regard to AQP2 trafficking, prior evidence for a role for PKA has been derived from the use of the protein kinase inhibitor H89 (44), which is known to inhibit several basophilic kinases other than PKA (26). Trafficking is governed by direct phosphorylation of AQP2, which is inhibited only by high, but not low (PKA-selective), concentrations of H89 (26). With regard to vasopressin-stimulated *Aqp2* gene transcription, our results suggest a direct role for PKA. A previous study used transgenic mice expressing a mutant PKA regulatory subunit (RIα) to create a dominant-negative phenotype with constitutively inactive PKA. Experiments in these mice did not demonstrate a change in AQP2 mRNA in collecting duct cells (45). It seems possible that PKA inactivation in these cells could have been incomplete or compartmentalized (46).

Materials and Methods

SI Materials and Methods includes a more detailed description of methods and materials.

Cell Lines. The immortalized mpkCCD line was produced in ref. 13 and recloned to maximize AQP2 abundance (15). mpkCCD cells were transfected with pCMV-Cas9-GFP plasmids containing gRNAs specific for *Prkaca* or *Prkacb* genes (Sigma), using Lipofectamine 3000 (Invitrogen) according to the manufacturer's instructions. GFP-expressing cells were sorted into 96-well plates (~1 cell per well) using a BD FACSAria II cell sorter for clone selection. Target gene expression was evaluated by Western blotting for PKA-Cα and PKA-Cβ, and the genomic indel mutations were identified by Sanger sequencing. To generate PKA double-knockout cells, PKA-Cβ knockout cells were transfected with the CRISPR-Cas9 plasmids targeting *Prkaca*. Control lines were made from cells that were carried through this protocol but continued to express both PKA genes (unmutated sequence confirmed by Sanger sequencing).

Cell Culture and Transient Transfection. Cells were maintained in either complete medium, DMEM/F-12 containing 2% serum and other supplements (5 μg/mL insulin, 50 nM dexamethasone, 1 nM triiodothyronine, 10 ng/mL epidermal growth factor, 60 nM sodium selenite, 5 μg/mL transferrin; all from Sigma), or simple medium (DMEM/F12 with dexamethasone, sodium selenite, and transferrin only). Except where indicated, cells were seeded on permeable membrane supports (Transwell) and grown on complete media containing 0.1 nM 1-desamino-8-D-arginine-vasopressin for 4 d. Then, the medium was changed to simple medium with 0.1 nM dDAVP and maintained for 3 d to ensure complete polarization. Transepithelial resistance was measured by EVOM (WPI), and growth medium was changed daily. For short-term vasopressin stimulation, dDAVP-conditioned cells were maintained in the absence of dDAVP for 2 h, and were then treated with either 0.1 nM dDAVP or vehicle for 30 min. In rescue and AQP2 trafficking experiments, the cells were transfected with plasmid vectors to express PKA-Cα, PKA-Cβ, or AQP2 (Sino Biological; MG50618-UT, MG50629-UT, or MG57478-UT) using Lipofectamine 3000. At the time of transfection, the cells were seeded on permeable supports and then grown to confluence.

Generation of Anti–PKA-Cα and –PKA-Cβ Antibodies. Peptides corresponding to amino acids 29 to 44 of mouse PKA-Cα (29-KKWETPSQNTAQLDQC-44) and PKA-Cβ (29-RKWENPPPSNAGLEDC-44) were synthesized, HPLC-purified, and conjugated to KLH. Rabbits were immunized using a standard protocol. Antibodies were affinity-purified using peptide affinity columns (Pierce; SulfoLink Kit). The antibodies' specificities were confirmed by dot blotting against the peptides, followed by Western blotting of cell homogenates from the PKA-Cα single knockout, PKA-Cβ single knockout, and PKA dKO cells.

Western Blotting and Nuclear Isolation. Cells were lysed with Laemmli buffer (1.5% SDS, 10 mM Tris, pH 6.8, protease and phosphatase inhibitors), and Western blotting was carried out as previously described (15). Nuclear and cytoplasmic extracts of scraped cells were prepared using the Nuclear Protein Extraction Kit (Thermo Fisher Scientific) following the manufacturer's instructions.

Immunofluorescence Microscopy. Cells were washed with PBS, fixed with 4% paraformaldehyde for 10 min, and permeabilized (0.1% BSA, 3% Triton X-100 in PBS) for 10 min. The cells were labeled as previously described (18) using primary antibodies (or phalloidin) as listed in Table S3. Confocal fluorescence images were obtained on an LSM 780 microscope (Zeiss).

SILAC Quantification of Proteins. The control cell lines were grown in culture medium containing $^{13}C_6$ $^{15}N_4$ arginine and $^{13}C_6$ lysine (heavy channel). PKA dKO cell lines were grown with $^{12}C_6$ $^{14}N_4$ arginine and $^{12}C_6$ lysine (light channel). The cells were cultured for 17 d (five passages) to reach >99.9% labeling efficiency (20). Heavy- or light-labeled cells were grown on permeable supports for 7 d in the presence of dDAVP (0.1 nM) in SILAC medium. Cells were lysed with 8 M urea and sonicated. Equal amounts (2 mg) of heavy and light protein extracts were mixed. The samples were reduced, alkylated, and diluted with 20 mM triethylammonium bicarbonate buffer (pH 8.5) to reduce urea to 1 M before digestion (trypsin/LysC; Promega). Peptides were desalted using hydrophilic–lipophilic–balanced extraction cartridges (Oasis), and fractionated with high-pH reverse-phase chromatography (Agilent; 1200 HPLC system). The fractions were split for total peptide analysis (2%) and phosphopeptide enrichment (49%, ×2), using either Fe-NTA or TiO_2 columns (Thermo Fisher Scientific). The enriched peptides were desalted using graphite columns, vacuum-dried, and stored at –80 °C. Peptides were resuspended with 0.1% formic acid before mass spectrometry analysis.

Total and phosphopeptides were analyzed using a Dionex UltiMate 3000 nano LC system connected to an Orbitrap Fusion ETD mass spectrometer equipped with an EASY-Spray ion source (Thermo Fisher Scientific). Peptides were introduced into a peptide nanotrap at a flow rate of 6 μL/min. The trapped peptides were fractionated with a reverse-phase EASY-Spray PepMap column (C18, 75 μm × 25 cm) using a linear gradient of 4 to 32% acetonitrile in 0.1% formic acid (120 min at 0.3 μL/min). MS spectra were analyzed using Proteome Discoverer 1.4. Peptide–spectra matching used both Mascot and SEQUEST. The mouse Swiss-Prot (July 10, 2016) database was used (false discovery rate < 0.01, peptide rank = 1). Relative quantification of peptides and phosphopeptides was performed using the quantification module within Proteome Discoverer 1.4, which calculates relative peptide abundance ratios from light and heavy channels using the areas under the curve for reconstructed MS1 ion chromatograms. Phosphorylation motifs were identified using PhosphoLogo (https://hpcwebapps.cit.nih.gov/PhosphoLogo/).

RNA Isolation and Sequencing. Total RNA was isolated from three biological replicates of PKA dKO and control cells using a Direct-zol RNA MiniPrep Plus Kit (Zymo Research) following the manufacturer's protocol. cDNA sequencing libraries were prepared from 260 ng of total RNA for each biological replicate using a TruSeq Stranded Total RNA Library Prep Kit after removal of rRNAs (Ribo-Zero rRNA Removal Kit; Illumina). The quality of the isolated total RNA and the synthesized cDNA was examined using an RNA 6000 Pico Kit (Agilent) and High Sensitivity DNA Analysis Kit (Agilent), respectively. Approximately 40 to 50 million 2 × 50-bp paired-end reads were sequenced by HiSeq 3000 (Illumina). Raw reads were mapped to mouse transcript sets (GRCm38.p5, comprehensive gene annotation) from GENCODE using STAR version 2.5.2a (default parameters). Read counts of genes were calculated using HOMER (4.8). The read counts were filtered (cpm > 4) and analyzed for differential expression between PKA dKO and control using default TMM (trimmed mean of M values) normalization within edgeR (3.10).

ChIP-Seq Analysis for Acetylated Histone H3K27. After treatment with dDAVP (0.1 nM) or vehicle for 24 h, cells were processed for ChIP using the truChIP Chromatin Shearing Reagent Kit (Covaris) following the manufacturer's protocol. Immunoprecipitations were carried out (SimpleChIP Chromatin IP Kit; Cell Signaling) using an anti-H3K27Ac antibody (Abcam; ab4729). Sheared chromatin was used as input control and anti-rabbit IgG was used as negative control in immunoprecipitation. Immunoprecipitated samples were incubated with proteinase K at 65 °C overnight. Gel-purified DNA fragments were used to prepare cDNA libraries using an Ovation Ultralow Library System (NuGen). Libraries (200 to 400 bp) were sequenced on a HiSeq 2000 platform (Illumina) to generate single-end 50-bp reads. The sequences were mapped to the mouse reference genome (mm10) using the Burrows–Wheeler Aligner.

Construction of a PKA Signaling Network. Protein kinases and phosphatases with phosphorylation sites that were significantly decreased or increased in abundance in PKA dKO cells were selected from the phosphoproteomic data. Among these, the phosphomodifications known to be associated with changes in enzymatic activity were identified using data from Kinexus PhosphoNET (www.phosphonet.ca/) and Signor 2.0 (signor.uniroma2.it/). These kinases were mapped to specific cellular processes using Gene Ontology Biological Process and Molecular Function terms. Those related to known regulatory actions of vasopressin in renal epithelial cells (Fig. 6*A*) were retained for further analysis. The known substrates of these kinases and phosphatases were identified using Kinexus PhosphoNET and by direct PubMed searches. These substrate phosphosites were mapped to the phosphoproteomic data for PKA dKO/controls generated in this paper, creating node–edge–node triplets representing elements of the network. These triplets were stitched together and tied to regulatory functions of vasopressin using prior data from the literature along with RNA-seq and histone H3K27Ac ChIP-seq data. The individual protein nodes of the network were annotated with prior information about their regulation in response to vasopressin in renal epithelial cells using *BIG* (https://big.nhlbi.nih.gov/index.jsp) (47) and from specific PubMed searches where appropriate. In the network, direct PKA phosphorylation target sites were assigned from SILAC phosphoproteomic data based on two criteria: (*i*) the presence of R or K in position –3 relative to the phosphorylated S or T, and (*ii*) phosphooccupancy of the site significantly decreased in PKA double-KO relative to control cells. Network visualization was achieved by creating a separate subnetwork for each functional response listed in Fig. 6*A* as separate but interlocking html files. The evidence for individual elements of the network is shown as mouse-over popups. The html files have been mounted on a permanent, publicly accessible website.

Statistical Analysis. Statistical methods are described in *SI Materials and Methods*.

Data Availability. Protein mass spectrometry data (raw files, search results, and spectra) have been uploaded to the ProteomeXchange Consortium via the PRIDE partner repository with the dataset identifier PXD005938. The FASTQ sequences and metadata for RNA-seq and ChIP-seq studies have been deposited in National Center for Biotechnology Information's Gene Expression Omnibus (GEO) database (accession no. GSE95009).

ACKNOWLEDGMENTS. This work was primarily funded by the Division of Intramural Research, National Heart, Lung, and Blood Institute (NHLBI) (Projects ZIA-HL001285 and ZIA-HL006129; to M.A.K.). The NHLBI Proteomics Core Facility (M. Gucek, Director), NHLBI DNA Sequencing Core Facility (Y. Li, Director), NHLBI Light Microscopy Core Facility (C. Combs, Director), and NHLBI Flow Cytometry Core Facility (P. McCoy, Director) were used. K.I. was supported by a Japan Society for the Promotion of Science Research Fellowship.

1. Rosenbaum DM, Rasmussen SG, Kobilka BK (2009) The structure and function of G-protein-coupled receptors. *Nature* 459:356–363.
2. Sutherland EW (1972) Studies on the mechanism of hormone action. *Science* 177:401–408.
3. Turnham RE, Scott JD (2016) Protein kinase A catalytic subunit isoform PRKACA; history, function and physiology. *Gene* 577:101–108.
4. Taylor SS, Zhang P, Steichen JM, Keshwani MM, Kornev AP (2013) PKA: Lessons learned after twenty years. *Biochim Biophys Acta* 1834:1271–1278.
5. Manning BD, Cantley LC (2002) Hitting the target: Emerging technologies in the search for kinase substrates. *Sci STKE* 2002:pe49.
6. Hutti JE, et al. (2004) A rapid method for determining protein kinase phosphorylation specificity. *Nat Methods* 1:27–29.
7. Miller ML, et al. (2008) Linear motif atlas for phosphorylation-dependent signaling. *Sci Signal* 1:ra2.
8. Douglass J, et al. (2012) Identifying protein kinase target preferences using mass spectrometry. *Am J Physiol Cell Physiol* 303:C715–C727.
9. Dinkel H, et al. (2011) Phospho.ELM: A database of phosphorylation sites—Update 2011. *Nucleic Acids Res* 39:D261–D267.
10. Goel R, Harsha HC, Pandey A, Prasad TS (2012) Human Protein Reference Database and Human Proteinpedia as resources for phosphoproteome analysis. *Mol Biosyst* 8:453–463.
11. Safaei J, Mañuch J, Gupta A, Stacho L, Pelech S (2011) Prediction of 492 human protein kinase substrate specificities. *Proteome Sci* 9:S6.
12. Hornbeck PV, Chabra I, Kornhauser JM, Skrzypek E, Zhang B (2004) PhosphoSite: A bioinformatics resource dedicated to physiological protein phosphorylation. *Proteomics* 4:1551–1561.
13. Duong Van Huyen J, Bens M, Vandewalle A (1998) Differential effects of aldosterone and vasopressin on chloride fluxes in transimmortalized mouse cortical collecting duct cells. *J Membr Biol* 164:79–90.
14. Gonin S, et al. (2001) Cyclic AMP increases cell surface expression of functional Na,K-ATPase units in mammalian cortical collecting duct principal cells. *Mol Biol Cell* 12:255–264.
15. Yu MJ, et al. (2009) Systems-level analysis of cell-specific AQP2 gene expression in renal collecting duct. *Proc Natl Acad Sci USA* 106:2441–2446.
16. Hasler U, et al. (2002) Long term regulation of aquaporin-2 expression in vasopressin-responsive renal collecting duct principal cells. *J Biol Chem* 277:10379–10386.
17. Sandoval PC, et al. (2013) Proteome-wide measurement of protein half-lives and translation rates in vasopressin-sensitive collecting duct cells. *J Am Soc Nephrol* 24:1793–1805.
18. Sandoval PC, et al. (2016) Systems-level analysis reveals selective regulation of Aqp2 gene expression by vasopressin. *Sci Rep* 6:34863.
19. Vuagniaux G, Vallet V, Jaeger NF, Hummler E, Rossier BC (2002) Synergistic activation of ENaC by three membrane-bound channel-activating serine proteases (mCAP1, mCAP2, and mCAP3) and serum- and glucocorticoid-regulated kinase (Sgk1) in *Xenopus* oocytes. *J Gen Physiol* 120:191–201.
20. Khositseth S, et al. (2011) Quantitative protein and mRNA profiling shows selective post-transcriptional control of protein expression by vasopressin in kidney cells. *Mol Cell Proteomics* 10:004036.
21. Ong SE, et al. (2002) Stable isotope labeling by amino acids in cell culture, SILAC, as a simple and accurate approach to expression proteomics. *Mol Cell Proteomics* 1:376–386.
22. Rinschen MM, et al. (2010) Quantitative phosphoproteomic analysis reveals vasopressin V2-receptor-dependent signaling pathways in renal collecting duct cells. *Proc Natl Acad Sci USA* 107:3882–3887.
23. Hoffert JD, Pisitkun T, Wang G, Shen RF, Knepper MA (2006) Quantitative phosphoproteomics of vasopressin-sensitive renal cells: Regulation of aquaporin-2 phosphorylation at two sites. *Proc Natl Acad Sci USA* 103:7159–7164.
24. Hoffert JD, et al. (2008) Vasopressin-stimulated increase in phosphorylation at Ser269 potentiates plasma membrane retention of aquaporin-2. *J Biol Chem* 283:24617–24627.
25. Xie L, et al. (2010) Quantitative analysis of aquaporin-2 phosphorylation. *Am J Physiol Renal Physiol* 298:F1018–F1023.
26. Bradford D, et al. (2014) Use of LC-MS/MS and Bayes' theorem to identify protein kinases that phosphorylate aquaporin-2 at Ser256. *Am J Physiol Cell Physiol* 307:C123–C139.
27. Yang CR, Raghuram V, Emamian M, Sandoval PC, Knepper MA (2015) Deep proteomic profiling of vasopressin-sensitive collecting duct cells. II. Bioinformatic analysis of vasopressin signaling. *Am J Physiol Cell Physiol* 309:C799–C812.
28. Hasler U, et al. (2006) Tonicity-responsive enhancer binding protein is an essential regulator of aquaporin-2 expression in renal collecting duct principal cells. *J Am Soc Nephrol* 17:1521–1531.
29. Li SZ, et al. (2007) Calcineurin-NFATc signaling pathway regulates AQP2 expression in response to calcium signals and osmotic stress. *Am J Physiol Cell Physiol* 292:C1606–C1616.
30. Luo C, et al. (1996) Recombinant NFAT1 (NFATp) is regulated by calcineurin in T cells and mediates transcription of several cytokine genes. *Mol Cell Biol* 16:3955–3966.
31. Soulsby MD, Wojcikiewicz RJ (2005) The type III inositol 1,4,5-trisphosphate receptor is phosphorylated by cAMP-dependent protein kinase at three sites. *Biochem J* 392:493–497.
32. Wojcikiewicz RJ, Luo SG (1998) Phosphorylation of inositol 1,4,5-trisphosphate receptors by cAMP-dependent protein kinase. Type I, II, and III receptors are differentially susceptible to phosphorylation and are phosphorylated in intact cells. *J Biol Chem* 273:5670–5677.
33. Henriksson E, et al. (2012) The AMPK-related kinase SIK2 is regulated by cAMP via phosphorylation at Ser358 in adipocytes. *Biochem J* 444:503–514.
34. Henriksson E, et al. (2015) SIK2 regulates CRTCs, HDAC4 and glucose uptake in adipocytes. *J Cell Sci* 128:472–486.
35. Bricambert J, et al. (2010) Salt-inducible kinase 2 links transcriptional coactivator p300 phosphorylation to the prevention of ChREBP-dependent hepatic steatosis in mice. *J Clin Invest* 120:4316–4331.
36. Altarejos JY, Montminy M (2011) CREB and the CRTC co-activators: Sensors for hormonal and metabolic signals. *Nat Rev Mol Cell Biol* 12:141–151.
37. Tie F, et al. (2009) CBP-mediated acetylation of histone H3 lysine 27 antagonizes *Drosophila* Polycomb silencing. *Development* 136:3131–3141.
38. Simon H, Gao Y, Franki N, Hays RM (1993) Vasopressin depolymerizes apical F-actin in rat inner medullary collecting duct. *Am J Physiol* 265:C757–C762.
39. Chou CL, et al. (2004) Non-muscle myosin II and myosin light chain kinase are downstream targets for vasopressin signaling in the renal collecting duct. *J Biol Chem* 279:49026–49035.
40. Nielsen S, et al. (1995) Vasopressin increases water permeability of kidney collecting duct by inducing translocation of aquaporin-CD water channels to plasma membrane. *Proc Natl Acad Sci USA* 92:1013–1017.
41. Gunaratne R, et al. (2010) Quantitative phosphoproteomic analysis reveals cAMP/vasopressin-dependent signaling pathways in native renal thick ascending limb cells. *Proc Natl Acad Sci USA* 107:15653–15658.
42. Pierce KL, Luttrell LM, Lefkowitz RJ (2001) New mechanisms in heptahelical receptor signaling to mitogen activated protein kinase cascades. *Oncogene* 20:1532–1539.
43. Nielsen S, et al. (2002) Aquaporins in the kidney: From molecules to medicine. *Physiol Rev* 82:205–244.
44. Brown D (2003) The ins and outs of aquaporin-2 trafficking. *Am J Physiol Renal Physiol* 284:F893–F901.
45. Gilbert ML, Yang L, Su T, McKnight GS (2015) Expression of a dominant negative PKA mutation in the kidney elicits a diabetes insipidus phenotype. *Am J Physiol Renal Physiol* 308:F627–F638.
46. Klussmann E, Rosenthal W (2001) Role and identification of protein kinase A anchoring proteins in vasopressin-mediated aquaporin-2 translocation. *Kidney Int* 60:446–449.
47. Zhao Y, Yang CR, Raghuram V, Parulekar J, Knepper MA (2016) BIG: A large-scale data integration tool for renal physiology. *Am J Physiol Renal Physiol* 311:F787–F792.